



# Adsorption of methyl blue, dichromate, and copper on ettringite under various pH values

Sarah Mariska<sup>1</sup> · Jr-Lin Lin<sup>2</sup> · Truong Thi Anh Tuyet<sup>3</sup> · Nguyen Duy Hai<sup>3,4</sup> · Huan-Ping Chao<sup>2,5</sup>

Received: 7 January 2024 / Accepted: 16 March 2024 / Published online: 10 April 2024  
© The Author(s) 2024

## Abstract

Ettringite is a hydrous calcium aluminum sulfate mineral present in cement. In this study, ettringite was synthesized via co-precipitation to remove methyl blue, dichromate, and copper ions from solutions with various pH values. The synthesized ettringite was characterized using scanning electron microscopy, X-ray photoelectron spectrometry, Fourier transform infrared spectroscopy, zeta potential analysis, and the Brunauer–Emmett–Teller method. Equilibrium adsorption experiments were performed using methyl blue and dichromate at pH values ranging from 5 to 11. To avoid precipitation, equilibrium adsorption experiments were performed on copper ions in solutions with pH values of 3, 4, and 5. The adsorption kinetics experiments for each contaminant were performed at pH 5. The results showed that ettringite was successfully synthesized, and calcite might have precipitated during the synthesis process. The point of zero charge was at pH 8.6. The maximum adsorption capacities for methyl blue, dichromate, and copper ions at pH 5 were 406, 321, and 365 mg/g, respectively. The adsorption kinetics fitted the pseudo-second-order model well. The properties of the contaminants affect their equilibrium and rate constants. Ion exchange is regarded as the primary adsorption mechanism, whereas the other mechanisms include complexation, hydrogen bonding, surface precipitation,  $\pi$ -interaction, and van der Waals forces. This study revealed a new adsorbent, ettringite, for the removal of contaminants from wastewater, which is a promising alternative adsorbent that can be used under specific conditions.

**Keywords** Ettringite · Methyl blue · Dichromate · Copper ion · Adsorption mechanism

## Introduction

Numerous contaminants are discharged into water bodies due to industrialization, urbanization, and population growth. Contaminants such as heavy metal ions and dyes can affect public health and ecosystems. Numerous methods have been developed to address this problem, including chemical precipitation, adsorption, photocatalysis, biological treatment, ion exchange, and membrane filtration (Price and Finney 2000; Liu et al. 2002; Pal et al. 2007). Biological treatment is considered to be a low-cost method. However, microorganisms cannot readily degrade all contaminants. Chemical precipitation is used to remove the specific contaminants. Photocatalysis, ion exchange, and membrane filtration are expensive operational techniques. Among these, adsorption is the most common method used to remove low concentrations of contaminants via advanced wastewater treatment.

Several other adsorbents have also been investigated. Zeolite, clay, and titanate nanotubes (TNTs) have been used

✉ Nguyen Duy Hai  
nguyenduyhai@tuaf.edu.vn

✉ Huan-Ping Chao  
hpchao@cycu.edu.tw

<sup>1</sup> Department of Civil, Chung Yuan Christian University, Taoyuan 32023, Taiwan

<sup>2</sup> Department of Environmental Engineering, Chung Yuan Christian University, Taoyuan 32023, Taiwan

<sup>3</sup> Faculty of Environment, Thai Nguyen University of Agriculture and Forestry (TUAF), Thai Nguyen City 24000, Vietnam

<sup>4</sup> Sustainable Technology and Solution Laboratory (STAS.Lab), Thai Nguyen University of Agriculture and Forestry (TUAF), Thai Nguyen City 24000, Vietnam

<sup>5</sup> Center for Environmental Risk Management, Chung Yuan Christian University, Taoyuan 32023, Taiwan

to remove cationic contaminants such as heavy metal ions and dyes (Lee et al. 2008; Motsi et al. 2009; Adeyemo et al. 2017). A cationic dye with a concentration of <30 mg/L can reach equilibrium kinetic adsorption within 30 min (Adeyemo et al. 2017). Activated carbon, biochar, and hydrochar have been used to adsorb organic compounds and heavy metal ions (Tran et al. 2017; Nguyen et al. 2019; Zhang et al. 2020). For example, the amounts of copper and cadmium adsorbed onto activated carbonaceous materials reached 182 and 208 mg/g, respectively (Nguyen et al. 2019). New carbonaceous materials such as carbon nanotubes, carbon spheres, and graphene oxide have been used as adsorbents to remove contaminants such as heavy metal ions, nonionic organic compounds, and dyes (Wang et al. 2009; Tofighy and Mohammadi 2011; Ranjan et al. 2019). Most adsorbents exhibit negatively charged surfaces. Therefore, these adsorbents do not easily adsorb anionic contaminants. Layered double hydroxides (LDHs) have been investigated for the adsorption of anionic contaminants, such as  $\text{AsO}_4^{3-}$ ,  $\text{Cr}_2\text{O}_7^{2-}$ ,  $\text{SeO}_3^{2-}$ ,  $\text{BrO}_3^-$ ,  $\text{PO}_4^{3-}$ ,  $\text{NO}_3^-$ , and dyes (Das et al. 2004; Goh et al. 2008; Yu et al. 2012; Chubar et al. 2013; Lei et al. 2017; Ji et al. 2017; Pourfaraj et al. 2017).

The surface properties of the adsorbents can determine the adsorbed amounts of contaminants. Several researchers have attempted to modify adsorbent surfaces, and these modified adsorbents can adsorb various types of contaminants. Cationic surfactant-modified zeolites, clays, and TNTs can absorb nonionic organic compounds, cationic metal ions, and oxyanions (Krishna et al. 2001; Chao et al. 2012; Orón-Navar et al. 2018). LDHs that are intercalated by organic acid can adsorb cationic and oxyanionic metals simultaneously (Tran et al. 2018). Although modified adsorbents can absorb more contaminants than their unmodified counterparts, they are rarely used for removing contaminants from wastewater. This is because the adsorbents release modified substances. To maintain the stability of the adsorbents, composite adsorbents have recently been developed to increase the adsorption amounts of specific contaminants or other types of contaminants (Begum et al. 2021; Zhang et al. 2022).

Although many adsorbents have been synthesized to remove different contaminants, some have not been comprehensively investigated. Herein, we present a novel ettringite adsorbent for cationic metal ions, oxyanions, and anionic dyes. Ettringite is a hydrous calcium aluminum sulfate mineral. The general molecular formula of ettringite is  $\text{Ca}_6\text{Al}_2(\text{SO}_4)_3(\text{OH})_{12}\cdot 26\text{H}_2\text{O}$  (Moore and Taylor 1968). Calcium ions and sulfate may form  $\text{CaSO}_4$ , and the remaining calcium ions can react with  $\text{H}_2\text{O}$  to form  $\text{Ca}\cdot 4\text{H}_2\text{O}$ . Meanwhile, aluminum ions generate coordinate bonds with the hydroxyl groups to form an octahedral structure.  $\text{Al}(\text{OH})_6^{3-}$  can bond with three  $\text{Ca}\cdot 4\text{H}_2\text{O}$  to form a polyhedron.  $\text{Al}(\text{OH})_6^{3-}$  in the polyhedron can connect with  $\text{Ca}\cdot 4\text{H}_2\text{O}$  in other polyhedra.

Ettringite typically forms rod-like crystals (Figure S1). Stacked aluminum and calcium hydroxide polyhedra were arranged along the crystallographic axis to form ettringite crystal structures. Hydroxyl groups were six times more abundant than aluminum ions along the central axis. The hydroxyl and  $\text{H}_2\text{O}$  molecules of the same structure, which appeared mainly around the central structure, produced ettringite. Additionally, these water molecules hydrate the hydration shells of intercolumnar sulfate ions (Tatarushkin et al. 2022). Ettringite can effectively adsorb anionic contaminants because it possesses the exchangeable anion  $\text{SO}_4^{2-}$ . Ettringite has been added to Portland cement to inhibit the release of toxic anions (Merlini et al. 2008). Therefore, the characteristics of ettringite in cement have been widely investigated (Cody et al. 2004; Tosun et al. 2010; Hargis et al. 2013; Shamaa et al. 2015). However, ettringite in low-pH solutions can generate unstable chemical structures. Several studies have used ettringite to adsorb anionic contaminants from water. Hiraga and Shigemoto (2010) used ettringite under specific conditions to remove borates. The borate removal rate increased with increasing amounts of  $\text{Ca}(\text{OH})_2/\text{Al}_2(\text{SO}_4)_3$ . Borate undergoes a co-precipitation reaction with  $\text{Al}(\text{OH})_3$  in a solution of pH 10. Iizuka et al. (2014) used ettringite derived from waste concrete to remove borate from water. However, they did not achieve high removal rates.

Ettringite was used in the present study to adsorb cationic and anionic contaminants. First, ettringite was synthesized via co-precipitation. Next, the characteristics of ettringite were determined by measuring its surface properties. The ettringite samples were prepared and used to adsorb copper ions, dichromate, and methyl blue (MB) at various pH values. Except for composite adsorbents, most adsorbents have only been applied to remove cationic or anionic contaminants. An alternative mineral, ettringite, which removes cationic and anionic contaminants from water and wastewater simultaneously, is presented herein.

## Materials and methods

### Materials and reagents

All chemicals with >95% purity were purchased from Merck or Sigma-Aldrich and used without further purification. Aluminum sulfate and calcium oxide were used to synthesize ettringite. Sulfuric acid and sodium hydroxide (NaOH) were used for pH adjustment. Stock solutions of MB, potassium dichromate, and copper nitrate were prepared. MB (anionic dye), dichromate, and copper ions were used as target contaminants.

## Synthesis of ettringite

First,  $\text{Ca}^{2+}/\text{Al}^{3+}/\text{SO}_4^{2-}$  with a molar ratio of 6:2:3 was used to prepare ettringite. Next, 138 g of CaO and 25.2 g of  $\text{Al}_2(\text{SO}_4)_3 \cdot 13\text{-}14\text{H}_2\text{O}$  were dissolved separately into 100 mL of distilled deionized (DD) water. After dissolving the chemicals in the DD water, the two solutions were mixed using a breaker. The pH of the solution was adjusted to 12. The mixture was then stirred at 25 °C for 6 h. The solution was filtered through a 0.45- $\mu\text{m}$  filter, and the solid was obtained. The ettringite samples were washed with DD water until the pH of the filtrate reached approximately 7.0, after which they were dried at 50 °C for 24 h to produce the adsorbent.

## Characterization of ettringite

The morphology of ettringite was determined using a field-emission scanning electron microscope (SEM; S-4800; Hitachi Ltd., Tokyo, Japan) and energy dispersive spectroscopy (EDS). EDS was used to determine the elemental composition of the samples. The crystal structures of ettringite samples were measured using X-ray diffraction (XRD; PW3040/60 X'Pert Pro, PANalytical, Worcestershire, UK) with Cu K $\alpha$  radiation ( $\alpha = 0.154$  nm). The scanning angle  $2\theta$  ranged from 5° to 60°, and the scanning rate was 3°/min. Fourier transform infrared (FTIR) spectra were obtained using a PerkinElmer (MA, USA) 1600 FTIR spectrophotometer to determine the functional groups. The pore characteristics and surface areas of the ettringite samples were determined using the Brunauer–Emmett–Teller (BET) method with a Micromeritics (GA, USA) ASAP 2020 sorptometer. The surface charges of the ettringite samples in a specified pH range were measured using a zeta potential analyzer (Zetasizer Nano-Z, Shimadzu, Kyoto, Japan).

## Equilibrium adsorption experiments

Equilibrium adsorption was performed using batch experiments. Each experiment was duplicated, the bias of the experiments exceeded 15%, and all experiments were performed in triplicate. Approximately 0.02 g of each adsorbent was added to a 50 mL Corex centrifuge tube containing the contaminant solution at concentrations ranging from 50 to 1000 mg/L. The pH of the solution was varied from 5 to 12. Because copper ions in high-pH solutions may generate precipitates, the pH values were set between 3 and 5 for copper ion adsorption. The centrifuge tubes were placed on a shaker at 150 rpm and 25 °C for 24 h to reach equilibrium. The solutions were filtered using a 0.45- $\mu\text{m}$  filter. The supernatants were obtained to measure the contaminant concentrations. The copper and dichromate concentrations were determined by atomic

absorption spectrometry (Avanta/AAS, GBC Scientific, Victoria, Australia). The MB concentration was determined using ultraviolet–visible (UV–vis) spectrophotometry (10 UV–vis, Genesys, CA, USA) at a wavelength of 633 nm. The amount of contaminant adsorbed at a specified concentration at equilibrium is expressed as  $q_e$  (mg/g), which can be calculated using the mass balance equation.

$$q_e = \frac{(C_o - C_e)}{m} V \quad (1)$$

where  $C_o$  (mg/L) and  $C_e$  (mg/L) are the initial and equilibrium concentrations of the adsorbates, respectively;  $m$  (g) is the mass of the adsorbent; and  $V$  (L) is the volume of each adsorbate solution.

To elaborate the adsorption characteristics of the test contaminants on ettringite, the Langmuir and Freundlich models are expressed as Eqs. (2) and (3), respectively.

$$q_e = \frac{Q_{\max} K_L C_e}{1 + K_L C_e} \quad (2)$$

$$q_e = K_F C_e^{1/n} \quad (3)$$

where  $q_e$  and  $C_e$  are defined in Eq. (1);  $Q_{\max}$  (mg/g) is the maximum adsorption capacity of the adsorbate on the adsorbent;  $K_L$  (l/mg) is the Langmuir constant; and  $K_F$  ((mg/g)/(mg/l)<sup>n</sup>) and  $n$  (dimensionless) are the Freundlich constants. All equilibrium adsorption experiments were performed in duplicate. When errors exceeded 15%, the experiments were performed in triplicate. The average values were used to estimate the model parameters.

## Experiments of adsorption kinetics

To investigate the adsorption kinetics, initial contaminant concentrations of 100, 300, and 500 mg/L were used. The pH of the solution was maintained at an optimum value for equilibrium adsorption experiments. Subsequently, 1.0 g of the adsorbent was added to 500 mL of the solution at 25 °C and 150 rpm using a magnetic stirrer. The samples were obtained at intervals of 0, 4, 16, 36, 64, 100, 144, 196, 256, 324, 400, and 1440 min. The obtained samples were filtered using a 0.22- $\mu\text{m}$  filter. Contaminant concentrations were analyzed using atomic absorption spectrometry or UV–vis spectrophotometry. The amount of contaminant adsorbed ( $q_t$ , mg/g) on the adsorbent at time  $t$  was calculated using Eq. (4).

$$q_t = \frac{(C_o - C_t)}{m} V \quad (4)$$

where  $C_o$  and  $C_t$  are the contaminant concentrations in the solution at the beginning and at any time, respectively;  $m$  (g) is the mass of the adsorbent; and  $V$  is the volume of the solution.

The nonlinear forms of the pseudo-first-order and pseudo-second-order models are expressed by Eq. (5) and (6), respectively.

$$q_t = q_e(1 - e^{-k_1 t}) \quad (5)$$

$$q_t = \frac{q_e^2 k_2 t}{1 + k_2 q_e t} \quad (6)$$

where  $k_1$  (1/min) and  $k_2$  (g/mg min) are the rate constants in the pseudo-first-order and pseudo-second-order equations, respectively. The adsorption kinetics experiments were performed in triplicate. The average values and error bars were used to express the error.

## Economic analysis

Adsorption is known to be a low-cost technology. The cost of an adsorbent to remove 1 g of adsorbate can be expressed as Eq. (7) (Pham et al. 2016). The total cost is calculated by the sum of purchased and energy costs. Equation (7) can be converted to Eq. (8).

$$\begin{aligned} & \text{adsorption cost for removing one gram contaminant} \\ &= \frac{\text{total cost (USD)}}{\text{removed contaminant (gram)}} \quad (7) \end{aligned}$$

$$\begin{aligned} & \text{Adsorption cost for removing one gram contaminant} \\ &= \frac{\left( \text{Chemical purchased cost} \left( \frac{\text{USD}}{\text{gram}} \right) + \text{Energy cost} \left( \frac{\text{USD}}{\text{gram}} \right) \text{ kWh} \right)}{\text{Adsorption capacity} \left( \frac{\text{mg}}{\text{g}} \right) \times 10^{-3} \frac{\text{g}}{\text{mg}}} \quad (8) \end{aligned}$$

## Results and discussion

### Properties of ettringite

SEM images of the synthetic ettringite are shown in Fig. 1. The synthetic ettringite displayed a rod-like appearance. Although ettringite may form ball and needle shapes (Tosun and Baradan 2010; Hargis et al. 2013), the rod shape is the most typical shape (Cody et al. 2004). The length of the ettringite was approximately 1  $\mu\text{m}$ . These results are consistent with those of a previous study (Mantellato et al. 2016).

To determine the main elemental composition of the synthetic ettringite, its EDS spectra were obtained, and the results are shown in Fig. S2. It primarily comprised oxygen, calcium, sulfur, and aluminum, which is consistent with the

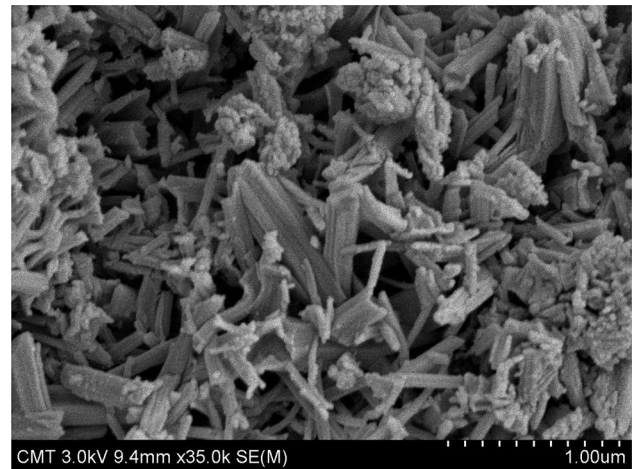


Fig. 1 SEM image of the synthetic ettringite

Table 1 Weight and mole ratios of the synthetic ettringite

Element	Weight ratio (%)	Molar ratio (%)
Ca	31.16	17.08
Al	6.99	5.68
S	13.26	9.08
O	45.25	62.06
C	3.34	6.10

elemental composition of ettringite. The trace amounts of carbon observed may have resulted from calcite ( $\text{CaCO}_3$ ), which is typically used in ettringite synthesis. The weight ratios of the elements measured using EDS are listed in Table 1. Owing to its chemical structure, oxygen exhibited the highest ratio in synthetic ettringite. The molar ratio of calcium/aluminum/sulfur was 6:2:3, which corresponded to the expected chemical structure of ettringite. Therefore, ettringite was successfully synthesized.

The XRD patterns of the synthesized samples are shown in Fig. 2. The XRD patterns showed that the synthesized samples possessed good crystallinity. The position of diffraction angles  $2\theta$  can reveal the crystal structure of the sample via a comparison between the “American Mineralogist Crystal Structure Database” and the literature (Clark and Brown 1999). The  $2\theta$  values of  $9.16^\circ$ ,  $15.73^\circ$ ,  $17.9^\circ$ ,  $18.86^\circ$ ,  $23.16^\circ$ ,  $25.66^\circ$ ,  $32.43^\circ$ , and  $35.1^\circ$  reflected the characteristic peaks of ettringite. The  $2\theta$  values at  $29.36^\circ$  and  $40.8^\circ$  were due to calcite. Because carbon dioxide in air may dissolve in the solution during synthesis, a high calcium concentration causes the precipitation of  $\text{CaCO}_3$ . This result was consistent with the aforementioned description of the weight ratios of the elements. The characteristic peaks of calcium sulfate ( $\text{CaSO}_4$ ) were located at  $2\theta = 14.68^\circ$ ,  $29.6^\circ$ ,  $32.04^\circ$ ,  $49.31^\circ$ , and  $54.08^\circ$ . However, the characteristic peaks of  $\text{CaSO}_4$  are

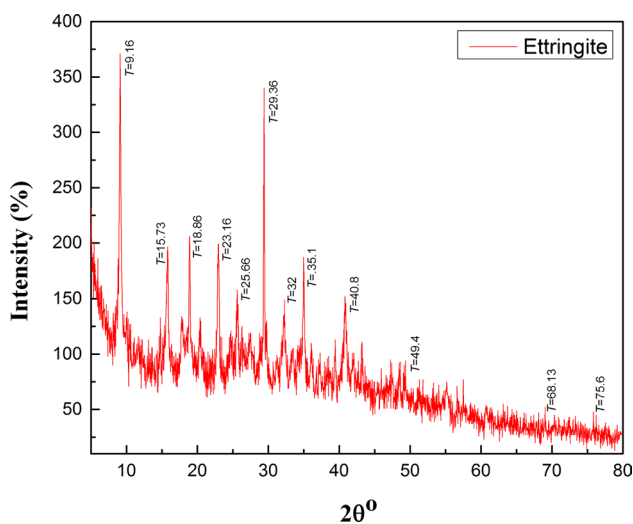


Fig. 2 XRD pattern of the synthetic ettringite

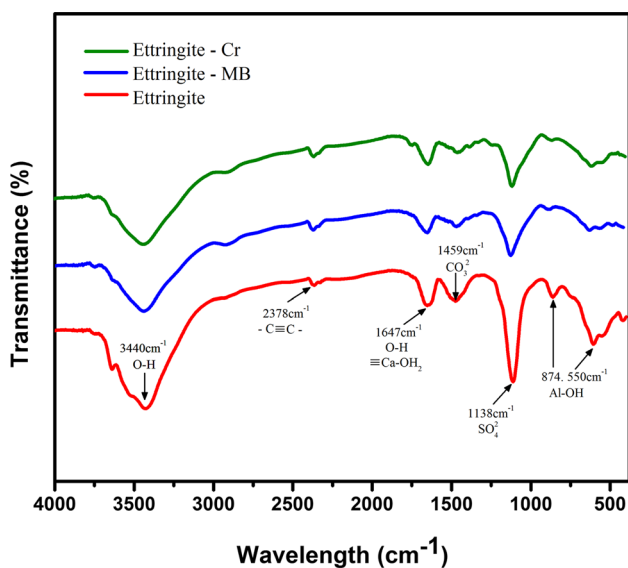


Fig. 3 FTIR spectra of the synthetic ettringite before and after adsorption

not shown in Fig. 2. The results revealed that although sulfate can react with calcium ions,  $\text{CaSO}_4$  is not released from ettringite to produce precipitation in the solution. However, the XRD patterns showed that ettringite was successfully synthesized.

The FTIR spectra of synthetic ettringite before and after adsorption are shown in Fig. 3. Before and after adsorption, the ettringite contained identical functional groups. The bands near  $3440\text{ cm}^{-1}$  were assigned to the O–H group, which is present in most minerals. The bands observed near  $1647\text{ cm}^{-1}$  were attributed to the bending vibration of  $\text{O–H}\equiv\text{Ca–OH}_2$ . The band at  $1138\text{ cm}^{-1}$  was attributed to the stretching vibration of  $\text{SO}_4^{2-}$ . The bands at  $874\text{ cm}^{-1}$  and

Table 2 The pore characteristics of the synthetic ettringite

	BET surface area ( $\text{m}^2/\text{g}$ )	Pore volume ( $\text{cm}^3/\text{g}$ )	Average pore size (nm)
Ettringite	14.2	0.108	30.2

$550\text{ cm}^{-1}$  corresponded to the bending vibration of Al–OH. These functional groups were consistent with the ettringite structure. The band at  $1459\text{ cm}^{-1}$  corresponded to the  $\text{CO}_3^{2-}$  group originating from  $\text{CaCO}_3$ , which is consistent with the XRD patterns.

Although the pore size, pore volume, and specific surface area of ettringite negligibly affected the adsorption capacities of the contaminants in this study, the pore characteristics of the adsorbent are important factors in determining the adsorption mechanisms of specific contaminants. For further observation of the pore characteristics, the adsorption–desorption isotherms of nitrogen for synthetic ettringite are illustrated in Fig. S3. The adsorption–desorption isotherms did not exhibit a significant hysteresis loop. According to the International Union of Pure and Applied Chemistry chemical nomenclature classification, the curve is a type-II isotherm. The results revealed that the synthetic ettringite without clear micropores was not a porous material. The pore size of the mesoporous materials does not limit the adsorption of dyes into the pores.

The pore characteristics included the BET specific surface area ( $S_{\text{BET}}$ ), average pore size, and pore volume (Table 2). The  $S_{\text{BET}}$  value of synthetic ettringite was  $14.2\text{ m}^2/\text{g}$ , which is slightly higher than that reported in the literature (Mantellato et al. 2016). The average pore size of  $30.2\text{ nm}$  shows that ettringite primarily comprised mesopores. A pore volume of  $0.108\text{ cm}^3/\text{g}$  is similar to that of minerals with mesopores.

The surface charge of ettringite varies with the solution pH. Surface charge is a key factor that affects contaminant adsorption through ion exchange. Figure 4 illustrates the measurement of the zeta potential of the synthetic ettringite in various pH solutions. As shown in Fig. 4, the zero charge sites of the synthetic ettringite occur at pH 8.6. A solution pH value  $>$  or  $<$  8.6 can affect the adsorption capacities of the test contaminants if ion exchange is regarded as the primary adsorption mechanism. A solution pH  $<$  8.6 favors the adsorption of MB and dichromate onto ettringite. A solution pH  $>$  8.6 favors the adsorption of copper ions on ettringite. However, in addition to ion exchange, other potential adsorption mechanisms may affect the adsorption capacity of the test contaminants. Therefore, the adsorption capacities of the test contaminants in solutions with various pH values must be determined.

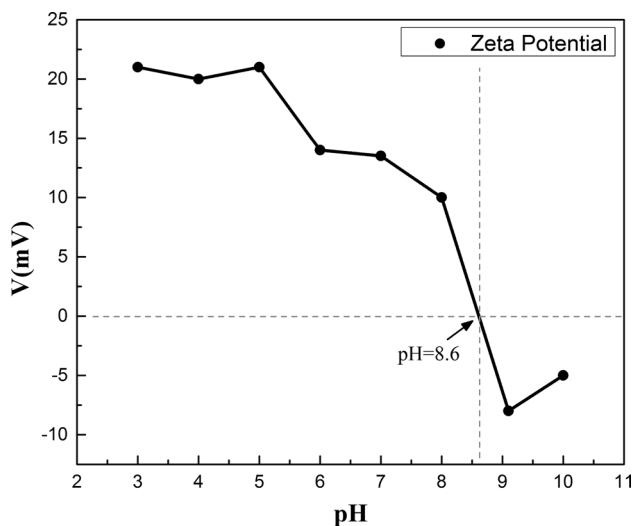


Fig. 4 Zeta potential of the synthetic ettringite

decreased as the pH of the solution increased. This occurred because OH<sup>-</sup> can compete with the anionic contaminants for adsorption sites. Moreover, H<sup>+</sup> competes with copper ions for adsorption sites. These results indicated that ion exchange was the primary adsorption mechanism. Synthetic ettringite with sulfate provides exchangeable anion sites for MB and dichromate. Calcium ions in ettringite can provide exchangeable cation sites for copper ions. In particular, when the solution pH exceeded 8.6, anionic contaminants were still adsorbed onto the ettringite. The results showed that other adsorption mechanisms were present between the anionic contaminants and ettringite.

The data fitting the Langmuir and Freundlich models for the adsorption of MB, dichromate, and copper ions on synthetic ettringite are presented in Tables 3, 4, and 5, respectively. The data fit the Langmuir model well, as indicated by the *R*-square values exceeding 0.95. The results showed that the maximum adsorption capacities for the test contami-

Table 3 Adsorption isotherm parameters of MB on the synthetic ettringite

pH	Langmuir model			Freundlich model		
	<i>Q</i> <sub>max</sub>	<i>R</i> <sup>2</sup>	<i>K</i> <sub>L</sub>	<i>R</i> <sup>2</sup>	<i>K</i> <sub>F</sub>	<i>n</i>
5	406	0.9769	0.0191	0.9495	18.1	3.98
6	388	0.9791	0.0126	0.9422	12.9	3.37
7	377	0.9629	0.0092	0.9626	12.1	3.13
8	349	0.9960	0.0075	0.9486	11.6	1.93
9	313	0.9837	0.0072	0.8609	5.23	1.58
10	273	0.9704	0.0092	0.7818	5.52	1.64
11	228	0.9650	0.0106	0.7609	6.56	1.81

### Equilibrium adsorption

The adsorption isotherms of the selected contaminants on synthetic ettringite in solutions with various pH values are shown in Figure S4. All isotherms displayed concave downward curves. The results show that synthetic ettringite is an excellent adsorbent for the selected contaminants in solutions with a pH of 3–11. For the anionic contaminants, MB and dichromate, the adsorption amounts increased as the solution pH decreased. The amount of copper adsorbed

nants could be estimated using the Langmuir model. All *n* values in the Freundlich model exceeded 1.0, which corresponded to the concave downward curves in the adsorption isotherms. As expected, the maximum adsorption capacities for MB and dichromate decreased in high-pH solutions. The *K*<sub>L</sub> values of the contaminants in the Langmuir model differed significantly. The *K*<sub>L</sub> values represent the ratios of the adsorption to desorption rates of the contaminants in the equilibrium state. The relatively high *K*<sub>L</sub> value indicates

Table 4 Adsorption isotherm parameters of dichromate on the synthetic ettringite

pH	Langmuir model			Freundlich model		
	<i>Q</i> <sub>max</sub>	<i>R</i> <sup>2</sup>	<i>K</i> <sub>L</sub>	<i>R</i> <sup>2</sup>	<i>K</i> <sub>F</sub>	<i>n</i>
5	321	0.9834	0.210	0.9158	11.5	3.29
6	308	0.9654	0.179	0.9321	18.3	3.33
7	252	0.9837	0.444	0.8705	18.7	3.81
8	218	0.9672	0.485	0.8940	10.6	3.90
9	202	0.9682	0.606	0.8784	9.5	4.09
10	185	0.9637	0.348	0.7506	14.5	3.61
11	171	0.9620	0.093	0.6432	10.9	2.59

**Table 5** Adsorption isotherm parameters of copper ion on the synthetic ettringite

pH	Langmuir model			Freundlich model		
	$Q_{max}$	$R^2$	$K_L$	$R^2$	$K_F$	$n$
3	213	0.9936	3.07	0.8820	18.2	8.41
4	267	0.9620	3.22	0.9316	15.1	7.93
5	365	0.9837	3.27	0.8091	13.7	4.93

a strong interaction between the adsorbate and adsorbent. From Tables 3, 4, 5, the  $K_L$  values, in the order of highest to lowest, are: MB < dichromate < copper. The results showed that the three contaminants interacted differently with synthetic ettringite.

The highest amounts of MB and dichromate adsorbed in the pH 5 solution were 406 and 321 mg/g, respectively. The adsorption amounts in this study are higher than those reported in the literature (Fan et al. 2012; Liu et al. 2013; Shu et al. 2015; Farahat et al. 2021; Tang et al. 2021; Xu et al. 2021). The highest amount of adsorbed copper ions was 365 mg/g. Copper ions can be adsorbed on the adsorbent through mechanisms other than ion exchange. Some adsorbents exhibited high adsorption capacities for copper ions. However, the adsorption amounts in this study were higher than those reported in the literature (Hansen et al. 2010; Demiral and Güngör, 2016; Nguyen et al. 2019). These results demonstrate that synthetic ettringite can effectively remove anionic and cationic contaminants from wastewater.

**Adsorption kinetics**

The maximum adsorption capacities for the selected contaminants were observed in solutions with pH 5. The adsorption kinetics curves for the three selected contaminants on ettringite in a pH 5 solution are shown in Fig. 5. The results show the adsorption kinetics of the three contaminants at initial concentrations ranging from 100 to 500 mg/L. The adsorption reactions of the three contaminants reached equilibrium within 100 min. The results showed that synthetic ettringite could rapidly remove contaminants when used for treating water or wastewater. The equilibrium times differed for the three contaminants. The adsorption reactions for MB, dichromate, and copper reached equilibrium after 100, 40–60, and 30–40 min, respectively. Because ettringite is not a porous material, the diffusion of the pores inside does not significantly affect the equilibrium time. These results were ascribed to differences in the adsorption mechanisms of the selected contaminants on the synthetic ettringite. Ion exchange was the primary mechanism by which dichromate and copper were absorbed by synthetic ettringite. The mechanism by which the MB absorbs synthetic ettringite is

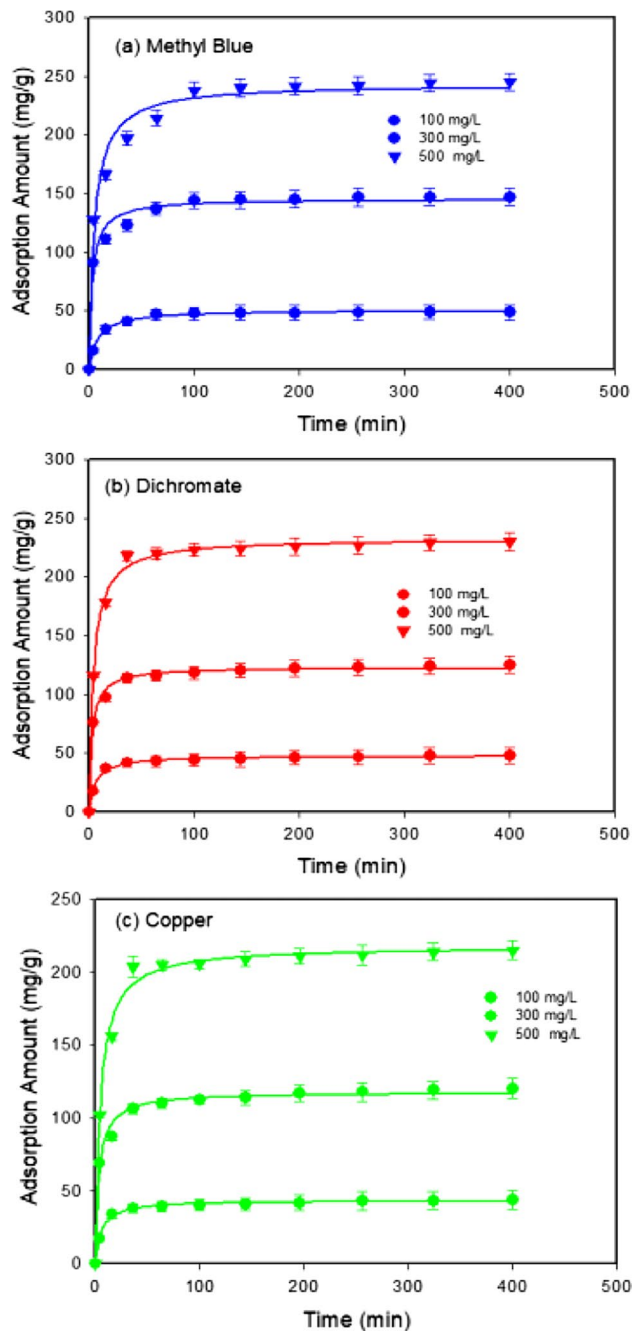


**Fig. 5** Adsorption kinetics of test contaminants (a-methyl blue; b-dichromate, and c-copper) on the synthetic ettringite

complex. In addition to ion exchange, hydrogen interactions, van der Waals forces, and other interactions are the potential adsorption mechanisms. The potential interactions are discussed in the subsequent sections.

The data for the adsorption kinetics of the three contaminants on synthetic ettringite fitted to the pseudo-first-order and pseudo-second-order models are listed in Table S1. The data fit the pseudo-second-order model well, as indicated by *R*-square values exceeding 0.999. These results support the previous assumption that chemical adsorption is the primary adsorption mechanism. The rate constants in the pseudo-second-order model decreased as the initial concentration increased. High contaminant concentrations significantly affected the adsorption rate. The rate constants for MB were significantly lower than those for dichromate and copper, which is consistent with previous descriptions of equilibrium time.

### Adsorption mechanisms

The crystal structure of ettringite varies with the solution pH. Metal ions may be partially released from ettringite in a low-pH solution to generate CaSO<sub>4</sub> (Hampson and Bailey 1982). However, synthetic ettringite generates significant amounts of adsorbed contaminants. The potential adsorption mechanism required further investigation. Copper ions are absorbed onto synthetic ettringite primarily through ion exchange. Copper can replace calcium in synthetic ettringite or CaSO<sub>4</sub> in low-pH solutions. However, hydrogen ions can compete with copper ions for adsorption sites. Thus, the number of copper ions adsorbed onto the synthetic ettringite increased with increasing solution pH. In addition, the complexation reaction was an important adsorption mechanism. The oxygen atoms in the synthetic ettringite may undergo complexation with the copper ions. Thus, the adsorption mechanisms of copper on synthetic ettringite were regarded as ion exchange and complexation reactions.

The adsorption mechanism of MB onto synthetic ettringite is complex. The potential adsorption mechanisms of dyes on the adsorbent include ion exchange, hydrogen bonding, surface precipitation,  $\pi$ -interaction, van der Waals force, and pore filling. Hydroxide ions competed with MB for adsorption sites. Ion exchange is regarded as an important adsorption mechanism. Calcium can attract anionic contaminants to the surface of an adsorbent and increase the adsorption of anionic contaminants. Thus, surface precipitation is a potential adsorption mechanism. The molecular formula of MB is C<sub>37</sub>H<sub>27</sub>N<sub>3</sub>Na<sub>2</sub>O<sub>9</sub>S<sub>3</sub>. Nitrogen, oxygen, and sulfur atoms can form hydrogen bonds with the oxygen atoms in ettringite. Therefore, hydrogen bonding is regarded as a potential pathway through which MB is adsorbed onto synthetic ettringite. However, hydrogen bonding only slightly increased the adsorption capacity. The

$\pi$  bond of the benzene ring on MB can generate a specific interaction with metals. MB with rich benzene rings can generate  $\pi$ -interactions with calcium and aluminum on the synthetic ettringite. Although the  $\pi$ -interaction with metal has previously been reported (Tran et al. 2016), the effect of the interaction on the adsorption amount has not been determined. Organic compounds with polar functional groups can also be adsorbed onto minerals (Chao et al. 2013). However, van der Waals forces are regarded as weak interactions between the organic compounds and ettringite. Ettringite, which lacks a large specific surface area, is not a porous material. Thus, the effect of van der Waals forces on the amount of MB adsorbed was negligible. Similarly, the effects of pore filling on adsorption were negligible.

Dichromate is an anionic contaminant that may replace the sulfate in synthetic ettringite. Calcium can attract dichromate to the surface of ettringite, increasing its adsorption amount. Ion exchange and surface precipitation are the potential mechanisms of adsorption.

### Adsorption cost

According to Eqs. (7) and (8), the adsorption costs of removing 1 g of MB, dichromate, and copper contaminants using ettringite were 0.63, 0.80 and 0.70 USD, respectively. The synthesis cost of ettringite is lower than that of adsorbents such as montmorillonite, TNTs, carbon spheres, and graphite oxide. However, these adsorbents have been used only to remove cationic contaminants. Ettringite can remove cationic and anionic contaminants simultaneously.

### Conclusion

In this study, ettringite was synthesized to adsorb MB, dichromate, and copper in solutions with various pH values. Although ettringite is rarely used as an adsorbent, synthetic ettringite can effectively remove anionic dyes, oxyanions, and cationic heavy metals from wastewater. The properties of ettringite varied with solution pH, and the maximum adsorption capacities for the selected contaminants were observed at pH 5. Ion exchange is regarded as the primary adsorption mechanism. Other mechanisms include complexation, hydrogen bonding, surface precipitation,  $\pi$ -interactions, and van der Waals forces. Based on the proposed mechanisms, synthetic ettringite has the potential to adsorb contaminants with similar properties. Therefore, if ettringite is utilized as an adsorbent for wastewater treatment, it could also be effective in treating other similar wastewater sources.



**Supplementary Information** The online version contains supplementary material available at <https://doi.org/10.1007/s13201-024-02161-y>.

**Funding** This work was supported by the grant MOST 111-2221-E-033-012- of Ministry of Science and Technology (Taiwan, ROC).

**Open Access** This article is licensed under a Creative Commons Attribution 4.0 International License, which permits use, sharing, adaptation, distribution and reproduction in any medium or format, as long as you give appropriate credit to the original author(s) and the source, provide a link to the Creative Commons licence, and indicate if changes were made. The images or other third party material in this article are included in the article's Creative Commons licence, unless indicated otherwise in a credit line to the material. If material is not included in the article's Creative Commons licence and your intended use is not permitted by statutory regulation or exceeds the permitted use, you will need to obtain permission directly from the copyright holder. To view a copy of this licence, visit <http://creativecommons.org/licenses/by/4.0/>.

## References

- Adeyemo AA, Adeoye IO, Bello OS (2017) Adsorption of dyes using different types of clay: a review. *Appl Water Sci* 7:543–568
- Begum S, Yuhana NY, Md Saleh N, Kamarudin NHN, Sulong AB (2021) Review of chitosan composite as a heavy metal adsorbent: Material preparation and properties. *Carbohydr Polym* 259:117613
- Chao H-P, Peng C-L, Lee C-K, Han Y-L (2012) A study on sorption of organic compounds with different water solubilities on octadecyltrichlorosilane-modified NaY zeolite. *J Taiwan Inst Chem Eng* 43:195–200
- Chao H-P, Lee C-K, Juang L-C, Han Y-L (2013) Sorption of organic compounds, oxyanions, and heavy metal ions on surfactant modified titanate nanotubes. *Ind Eng Chem Res* 52:9843–9850
- Chubar N, Gerda V, Megantari O, Micusík M, Omastova M, Heister K, Man P, Fraissard J (2013) Applications versus properties of Mg-Al layered double hydroxides provided by their syntheses methods: alkoxide and alkoxide-free sol-gel syntheses and hydrothermal precipitation. *Chem Eng J* 234:284–299
- Clark B, Brown PJC (1999) The formation of calcium sulfoaluminate hydrate compounds: part I. *Cem Concr Res* 29:1943–1948
- Cody AM, Lee H, Cody RD, Spry PG (2004) The effects of chemical environment on the nucleation, growth, and stability of ettringite  $[\text{Ca}_3\text{Al}(\text{OH})_6]_2(\text{SO}_4)_3 \cdot 26\text{H}_2\text{O}$ . *Cem Concr Res* 34:869–881
- Das NN, Konar J, Mohanta MK, Srivastava SC (2004) Adsorption of Cr(VI) and Se(IV) from their aqueous solutions onto Zr<sup>4+</sup>-substituted ZnAl/MgAl-layered double hydroxides: effect of Zr<sup>4+</sup> substitution in the layer. *J Colloid Interface Sci* 270:1–8
- Demiral H, Güngör C (2016) Adsorption of copper(II) from aqueous solutions on activated carbon prepared from grape bagasse. *J Clean Prod* 124:103–113
- Fan L, Luo C, Li X, Lu F, Qiu H, Sun M (2012) Fabrication of novel magnetic chitosan grafted with graphene oxide to enhance adsorption properties for methyl blue. *J Hazard Mater* 215:272–279
- Farahat MM, Sanad MM, Abdel-khalek MJPT (2021) Decoration of serpentine with iron ore as an efficient low-cost magnetic adsorbent for Cr(VI) removal from tannery wastewater. *Powder Technol* 388:51–62
- Goh K-H, Lim T-T, Dong Z (2008) Application of layered double hydroxides for removal of oxyanions: a review. *Water Res* 42:1343–1368
- Hampson CJ, Bailey JE (1982) On the structure of some precipitated calcium aluminosulfate hydrates. *J Mater Sci* 17:3341–3346
- Hansen HK, Arancibia F, Gutiérrez C (2010) Adsorption of copper onto agriculture waste materials. *J Hazard Mater* 180:442–448
- Hargis CW, Kirchheim AP, Monteiro PJM, Gartner EM (2013) Early age hydration of calcium sulfoaluminate (synthetic ye'elimite,  $\text{C}_4\text{A}_3\text{S}$ ) in the presence of gypsum and varying amounts of calcium hydroxide. *Cem Concr Res* 48:105–115
- Hiraga Y, Shigemoto N (2010) Boron uptake behavior during ettringite synthesis in the presence of  $\text{H}_3\text{BO}_3$  and in a suspension of ettringite in  $\text{H}_3\text{BO}_3$ . *J Chem Eng Jpn* 43:865–871
- Iizuka A, Takahashi M, Nakamura T, Yamasaki A (2014) Boron removal performance of a solid sorbent derived from waste concrete. *Ind Eng Chem Res* 53:4046–4051
- Ji H, Wu W, Li F, Yu X, Fu J, Jia L (2017) Enhanced adsorption of bromate from aqueous solutions on ordered mesoporous Mg-Al layered double hydroxides (LDHs). *J Hazard Mater* 334:212–222
- Krishna BS, Murty DSR, Prakash BSJ (2001) Surfactant-modified clay as adsorbent for chromate. *Appl Clay Sci* 20:65–71
- Lee C-K, Wang C-C, Juang L-C, Lyu M-D, Hung S-H, Liu S-S (2008) Effects of sodium content on the microstructures and basic dye cation exchange of titanate nanotubes. *Colloids Surf A Physicochem Eng Asp* 317:164–173
- Lei C, Zhu X, Zhu B, Jiang C, Le Y, Yu J (2017) Superb adsorption capacity of hierarchical calcined Ni/Mg/Al layered double hydroxides for Congo red and Cr(VI) ions. *J Hazard Mater* 321:801–811
- Liu R, Guo J, Tang H (2002) Adsorption of fluoride, phosphate, and arsenate ions on a new type of ion exchange fiber. *J Colloid Interface Sci* 248:268–274
- Liu R, Shen X, Yang X, Wang Q, Yang F (2013) Adsorption characteristics of methyl blue onto magnetic  $\text{Ni}_{0.5}\text{Zn}_{0.5}\text{Fe}_2\text{O}_4$  nanoparticles prepared by the rapid combustion process. *J Nanopart Res* 15:1679–1690
- Mantellato S, Palacios M, Flatt RJ (2016) Impact of sample preparation on the specific surface area of synthetic ettringite. *Cem Concr Res* 86:20–28
- Merlini M, Artioli G, Cerulli T, Cella F, Bravo A (2008) Tricalcium aluminate hydration in additivated systems. A crystallographic study by SR-XRPD. *Cem Concr Res* 38:477–486
- Moore A, Taylor HFW (1968) Crystal structure of ettringite. *Nature* 218:1048–1049
- Motsi T, Rowson NA, Simmons MJH (2009) Adsorption of heavy metals from acid mine drainage by natural zeolite. *Int J Miner Process* 92:42–48
- Nguyen HD, Tran HN, Chao H-P, Lin C-C (2019) Activated carbons derived from teak sawdust-hydrochars for efficient removal of methylene blue, copper, and cadmium from aqueous solution. *Water* 11:2581–2597
- Orona-Navar C, Garcia-Morales R, Rubio-Govea R, Mahlkecht J, Hernandez-Aranda RI, Ramirez JG, Nigam KDP, Ornelas-Soto N (2018) Adsorptive removal of emerging pollutants from groundwater by using modified titanate nanotubes. *J Environ Chem Eng* 6:5332–5340
- Pal P, Ahammad SZ, Pattanayak A, Bhattacharya P (2007) Removal of arsenic from drinking water by chemical precipitation – A modeling and simulation study of the physical-chemical processes. *Water Environ Res* 79:357–366
- Pham T-H, Lee B-K, Kim J (2016) Improved adsorption properties of a nano zeolite adsorbent toward toxic nitrophenols. *Process Saf Environ Prot* 104:314–322
- Pourfaraj R, Fatemi SJ, Kazemi SY, Biparva P (2017) Synthesis of hexagonal mesoporous MgAl LDH nanoplatelets adsorbent for the effective adsorption of Brilliant Yellow. *J Colloid Interface Sci* 508:65–74

- Price CP, Finney H (2000) Developments in the assessment of glomerular filtration rate. *Clin Chim Acta* 297:55–66
- Ranjan P, Balakrishnan J, Thakur AD (2019) Dye adsorption behavior of graphene oxide. *Mater Today: Proc* 11:833–836
- Al Shamaa M, Lavaud S, Divet L, Nahas G, Torrenti JM (2015) Influence of relative humidity on delayed ettringite formation. *Cem Concr Compos* 58:14–22
- Shu Y, Shao Y, Wei X, Wang X, Sun Q, Zhang Q, Li L (2015) Synthesis and characterization of Ni-MCM-41 for methyl blue adsorption. *Microporous Mesoporous Mater* 214:88–94
- Tang J, Zhao B, Lyu H, Li D (2021) Development of a novel pyrite/biochar composite (BM-FeS<sub>2</sub>@ BC) by ball milling for aqueous Cr (VI) removal and its mechanisms. *J Hazard Mater* 413:125415
- Tararushkin EV, Pisarev VV, Kalinichev AG (2022) Atomistic simulations of ettringite and its aqueous interfaces: Structure and properties revisited with the modified ClayFF force field. *Cem Concr Res* 156:106759
- Tofighy MA, Mohammadi T (2011) Adsorption of divalent heavy metal ions from water using carbon nanotube sheets. *J Hazard Mater* 185:140–147
- Tosun K, Baradan BJC, Composites C (2010) Effect of ettringite morphology on DEF-related expansion. *Cem Concr Compos* 32:271–280
- Tran HN, You S-J, Chao H-P (2016) Effect of pyrolysis temperatures and times on the adsorption of cadmium onto orange peel derived biochar. *Waste Manag* 34:129–138
- Tran HN, Lee C-K, Vu MT, Chao H-P (2017) Removal of copper, lead, methylene green 5, and acid red 1 by saccharide-derived spherical biochar prepared at low calcination temperatures: adsorption kinetics, isotherms, and thermodynamics. *Water Air Soil Pollut* 228:401–416
- Tran HN, Lin C-C, Chao H-P (2018) Amino acids-intercalated Mg/Al layered double hydroxides as dual-electronic adsorbent for effective removal of cationic and oxyanionic metal ions. *Sep Purif Technol* 192:36–45
- Wang Q, Liang X, Qiao W, Liu C, Liu X, Zhan L, Ling L (2009) Preparation of polystyrene-based activated carbon spheres with high surface area and their adsorption to dibenzothiophene. *Fuel Process Technol* 90:381–387
- Xu H, Gao M, Hu X, Chen Y, Li Y, Xu X, Zhang R, Yang X, Tang C, Hu X (2021) A novel preparation of S-nZVI and its high efficient removal of Cr (VI) in aqueous solution. *J Hazard Mater* 416:125924
- Yu X-Y, Luo T, Jia Y, Xu R-X, Gao C, Zhang Y-X, Liu J-H, Huang X-J (2012) Three-dimensional hierarchical flower-like Mg-Al-layered double hydroxides: highly efficient adsorbents for As(v) and Cr(vi) removal. *Nanoscale* 4:3466–3474
- Zhang J-W, Nur'aini AD, Wang Y-C, Nguyen DH, Minh DV, Chao H-P (2022) Multiple pollutants removal by carbon sphere and layered double hydroxide composites: adsorption behavior and mechanisms. *J Environ Chem Eng* 10:108014
- Zhang XB, Zhang YC, Ngo HH, Guo WS, Wen HT, Zhang D, Li CC, Qi L (2020) Characterization and sulfonamide antibiotics adsorption capacity of spent coffee grounds based biochar and hydrochar. *Sci Total Environ* 716:137015

**Publisher's Note** Springer Nature remains neutral with regard to jurisdictional claims in published maps and institutional affiliations.